ADVANCED FUNCTIONAL MATERIALS
www.afm-journal.de

Self-Assembly of Multiple Stacked Nanorings by Vertically Correlated Droplet Epitaxy

Jiang Wu, Yusuke Hirono, Xinlei Li, Zhiming M. Wang, Jihoon Lee, Mourad Benamara, Siyuan Luo, Yuriy I. Mazur, Eun Soo Kim, and Gregory J. Salamo*

Fabrication of advanced artificial nanomaterials is a long-term pursuit to fulfill the promises of nanomaterials. In the last ten years, droplet epitaxy has been emerging as a versatile fabrication method for various complex nanomaterials, but there is a lack of growth protocol to control the growth vertically. Here we report a vertically correlated droplet epitaxy growth method. We find that the nanodroplets form preferable on the preexisting nanorings, which enables fabrication of vertically aligned nanostructures by droplet epitaxy. Nucleation thermodynamics and growth kinetics have been proposed to explain the vertically correlated droplet epitaxy. Heterojunctions can be realized at nanoscale by the presented method. In addition, the nucleation thermodynamics of nanodroplets observed in this article will allow site-controlled fabrication of nanostructures.

1. Introduction

Quantum structures have been of significant interest for many years due to their appealing properties arising from different degrees of quantum confinement. For example, quantum dots, often referred to as "artificial atoms", have great potential for creating state-of-the-art solar cells,[1] single photon sources,[2] photodetectors,[3] lasers,[4] and quantum qubits[5,6] due to their tunable discrete energy levels and long carrier lifetimes. A lot of effort has been devoted to creating and manipulating materials at nanoscale to meet urgent demands of quantum structures with designed properties. Many complex quantum structures, including core–shell quantum dots (QDs),[7] QD molecules,[8] nanowires,[9] and quantum rings,[10] were demonstrated thanks to advances in epitaxial growth techniques. In particular, the recent developments of droplet epitaxy attracted significant attention for the self assembly of quantum structures. Droplet epitaxy is a growth method which creates semiconductor nanostructures through crystallization of metallic nanodroplets by supplying source elements in an alternating way. Due to the unique growth protocols, droplet epitaxy is capable of forming various complex quantum structures on both lattice-mismatched and lattice-matched material systems, including multiple quantum rings, quantum dot pairs, and quantum dot disks.[10–13] In addition, three-dimensional control of quantum dot clusters was enabled by combining the droplet epitaxy technique and the conventional Stranski–Krastanov (S–K) growth mode.[14–16]

Generally, droplet epitaxy is a flexible nanostructure fabrication technique that is applicable to a wide range of materials and able to control and design complex semiconductor nanostructures by choosing the proper growth conditions. The main strategy for fabricating nanostructures using droplet epitaxy is to precisely control the lateral diffusion and crystallization processes. However, the growth control of nanomaterials in the vertical or growth direction is less explored for droplet epitaxy. Unlike S–K quantum dots, formed through strain-driven self-organization, where vertical correlation is naturally available between adjacent quantum dot layers through the strain field,[17,18] lattice-matched nanostructures fabricated by droplet epitaxy lack a mechanism to couple neighboring layers. Droplet epitaxy has been successfully employed in fabricating various kinds of nanostructures such as multiple quantum rings and nanoholes that are not easily obtainable by S–K growth mode,[10,19] while a vertical growth protocol of droplet epitaxy would add another dimension of control in fabricating advanced nanostructures.

We report a method to grown vertically stacked quantum rings using droplet epitaxy. In previous reports, quantum

Dr. J. Wu, Prof. Z. M. Wang, S. Luo
State Key Laboratory of Electronic Thin Films and Integrated Devices
University of Electronic Science and Technology of China
Chengdu, 610054, PR China
E-mail: zhmwang@uestc.edu.cn
Y. Hirono, Prof. Z. M. Wang, Dr. M. Benamara, Dr. Y. I. Mazur, Prof. E. S. Kim, Prof. G. J. Salamo
Arkansas Institute for Nanoscale Materials Science and Engineering
University of Arkansas
Fayetteville, AR 72701, USA
Dr. X. Li
MOE Key Laboratory of Laser Life Science & Institute of Laser Life Science
College of Biophotonics
South China Normal University
Guangzhou, 510631, PR China
Dr. J. Wu
Department of Electronic and Electrical Engineering
University College London, Torrington Place
London, WC1E 7JE, UK
Dr. J. H. Lee, Prof. E. S. Kim
College of Electronics and Information
Kwangwoon University
Nowon-gu, Seoul, 139–701, South Korea

DOI: 10.1002/adfm.201302032

structures grown by droplet epitaxy were separated by spacer layers, which are grown under conventional growth conditions. In the absence of strain in lattice-mismatched materials, vertical alignment between adjacent quantum structure layers cannot be obtained. In this article, nanodroplets have been observed to nucleate over preceding nanocrystals formed by droplet epitaxy. The nanocrystals serve as preferred nucleation sites of subsequent nanodroplets for both homo- and heteroepitaxy. As a result, multiple stacked GaAs/AlGaAs nanorings can be fabricated by alternatively depositing GaAs and AlGaAs layers using droplet epitaxy.

2. Results and Discussion

2.1. Vertically Correlated Homo-Droplet Epitaxy and Nucleation Thermodynamics

The vertically correlated multiple-deposition droplet epitaxy processes for fabricating the stacked GaAs/AlGaAs nanorings is introduced. First, three samples were grown: (a) Ga nanodroplets with an equivalent amount of three monolayer (ML) GaAs coverage was deposited on sample A; (b) same amount Ga is supplied to form nanodroplets on sample B and the nanodroplets were crystallized in nanorings under As_4 flux (beam equivalent pressure (BEP) of 1.2×10^{-5} Torr); (c) after formation of same GaAs nanorings as sample B, the As cell shutter was closed again. The growth was paused for 10 min to reduce the As background pressure and then a second deposition of 3 ML Ga was carried out on sample C (see the Supporting Information for detailed methods.) **Figure 1** shows the atomic force microscopy (AFM) images of the surface morphology for samples A, B and C. Typically, the Ga nanodroplets are formed on the GaAs surface when Ga molecular beam is supplied in an As-depleted environment, as shown in Figures 1(a) and (d1). After forming Ga nanodroplets, a molecular beam is immediately supplied to crystallize the Ga nanodroplets into GaAs nanorings, as shown in Figures 1(b) and (d2). The design and control of fabricating nanodroplets and nanorings have been well documented in previous reports.[10,13] Interestingly, Ga nanodroplets tend to nucleate right over the GaAs nanorings with a second deposition of Ga in the As-depleted environment. Figures 1(c) and (d3) show the nanodroplet/nanoring hybrid structures. The Ga nanodroplets are observed to form on the GaAs nanorings. The direct nucleation of nanodroplets on the preexisting nanorings is intriguing because more complex nanostructures can be designed and fabricated by droplet epitaxy.

Here, we apply the nucleation thermodynamics of droplets to understand the vertically correlated nucleation of nanodroplets. From the views of thermodynamics, we can compare the energy barrier of each nucleation site to clarify which site is the most energetically favorable. Based on the surface morphology of the formed GaAs nanorings, we define θ as the angle between the nanostructure and substrate surface. As shown in the inset of Figure 1e, the nanostructure represents a concave surface structure when $\theta > 0$ (convex when $\theta < 0$). Based the nucleation thermodynamics, the dependence of ΔG^* on the angle θ can be expressed as

$$\Delta G^* = -\frac{32\gamma_{lv}^3 f_1^3(\theta, \alpha)}{27 g_v^2 f_2^2(\theta, \alpha)} \quad (1)$$

where γ_{lv} represents the surface energy density of Ga droplet, α is the contact angle of droplet with substrate surface, g_v is the Gibbs free energy per unit volume, $f_1(\theta, \alpha)$ and $f_2(\theta, \alpha)$ are geometric factors (see the Supporting Information for

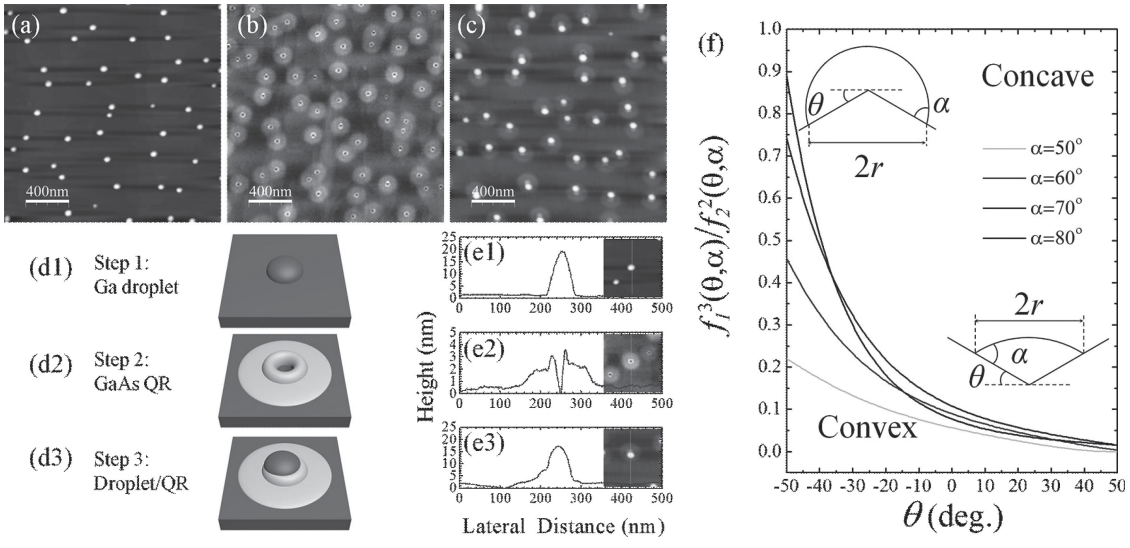

Figure 1. AFM images of Ga nanodroplets on sample A (a), GaAs nanorings on sample B (b), and Ga nanodroplets formed on GaAs nanorings on sample C. Illustration of forming Ga nanodroplets (d1), GaAs nanorings (d2), and nanodroplet/nanoring hybrids (d3) on samples A, B, and C, respectively. AFM line profiles of a single Ga nanodroplet (e1), GaAs nanoring (e2), and nanodroplet/nanoring hybrid (e3). The profiles taken along the lines indicated in insets of (e1–e3). (f) The dependence of $f_1^3(\theta, \alpha)/f_2^2(\theta, \alpha)$ on the angle θ. The calculation assumes that the contact angle α is equal to a set of different values: 50°, 60°, 70°, and 80°. The insets illustrate the nanodroplets formed on convex and concave surfaces.

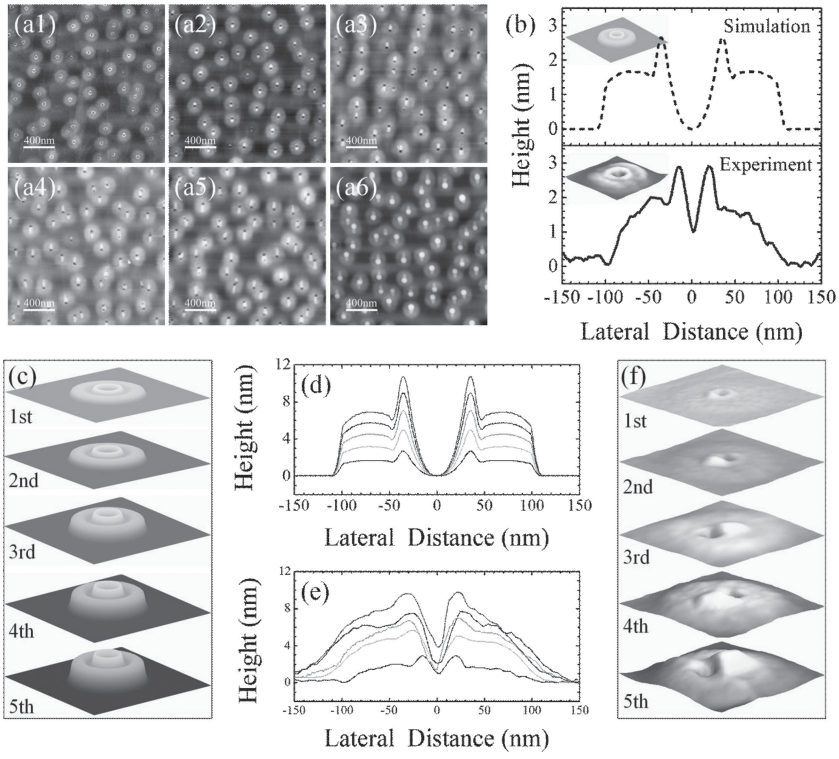

Figure 2. AFM images of the nanorings with one deposition cycle (sample B) (a1), two cycles (sample D) (a2), three cycles (sample E) (a3), four cycles (sample F) (a4), five cycles (sample G) (a5), and nanorings with five deposition cycles and an additional deposition of nanodroplets (sample H) (a6). (b) Simulation and experiment results of a single layer quantum ring. The insets are the simulated nanoring and measured nanoring AFM image. Simulation results(c)-(d) and AFM measurements (e,f) of final shapes of GaAs after different deposition cycles under growth temperature of 280 °C and BEP of 1.2×10^{-5} Torr. (c) and (d) are the simulated three dimension surface morphologies of the final shapes of GaAs nanorings after different deposition cycles. (e) and (f) are the cross-sectional height profiles obtained from simulated results and AFM images. The initial radius of Ga droplet is 40 nm. The AFM line profiles are taken along the [011] direction.

a detailed derivation). Given that γ_{lv} and g_v are constants determined by material properties, ΔG^* is mainly dependent on $f_1^3(\theta,\alpha)/f_2^2(\theta,\alpha)$. The dependence of $f_1^3(\theta,\alpha)/f_2^2(\theta,\alpha)$ on the angle θ is plotted in Figure 1. One clearly sees that $f_1^3(\theta,\alpha)/f_2^2(\theta,\alpha)$ decreases as the angle θ increases.[20] Thus, these observations show that ΔG^* also decreases with increasing θ, and the energy barrier of the critical nucleus on a concave surface is therefore generally smaller than that of the critical nucleus on the convex and flat surfaces. Therefore, instead of nucleating on the surface of a GaAs nanoring, the Ga nanodroplets favor nucleating in the center of nanorings where angle θ is the largest. In addition, the nanosized hole formed in the center of the nanoring is elongated in the $[01\bar{1}]$ direction due to anisotropic diffusion, which has made the nanodroplets on the nanorings slightly off-center along the $[01\bar{1}]$ direction, as shown in Figure 1(e3).

Figures 1(e1–e3) shows the AFM line profiles taken along the $[01\bar{1}]$ direction. The height line scans taken from the AFM images are indicated in the insets of Figures 1(e1–e3). The height of the example nanodroplet, nanoring, and nanodroplet/nanoring hybrid is 19.5 nm, 3.6 nm for inner ring (2.0 nm for outer ring), and 17.5 nm, respectively. With the second deposition of Ga nanodroplets, the initial nanorings become flatter which is caused by lateral diffusion of atoms during growth pause. The nanodroplets on the nanorings are also shorter than those formed on the atomic flat GaAs surface because of change of the surface roughness. Wenzel described the relationship between the surface roughness and contact angle as[21,22]

$$\cos\alpha_R = R\cos\alpha \quad (2)$$

where α and α_R is the contact angle of a droplet on a smooth surface and rough surface, respectively, and R is the roughness factor. When the contact angle is smaller than 90°, an increase in surface roughness results in a decrease in the contact angle.

2.2. Growth and Simulation of Multiple Stacked Nanorings by Droplet Epitaxy

To confirm the possibility for vertical stacking of GaAs nanorings using droplet epitaxy, additional five samples were fabricated: for the first four samples (D, E, F, and G), the nanoring growth steps of sample B (depletion of As, Ga deposition, and crystallization) were repeated for 2, 3, 4, and 5 cycles; another sample, labeled H, includes 5 cycles of nanorings and an additional deposition of 3 ML Ga droplets. **Figure 2** shows the AFM images of samples B, D, E, F, G, and H. It is shown that the increase of deposition cycles doesn't change significantly the shape of the nanorings. Figure 2(a1–a5) reveals that reveals that the similar nanorings are formed with increasing deposition cycles. Figure 2(a6) shows an AFM image of sample H. Like sample C, the Ga nanodroplets are observed to form on the GaAs nanorings which was fabricated with five cycles of depositions on sample H. The localized nucleation of nanodroplets indicates that nanostructure fabrication can be designed and controlled in the growth direction using multiple droplet homo-epitaxy depositions.

In order to provide a much more comprehensive and descriptive view of the formation of vertically stacked quantum rings, the final shapes of GaAs after different deposition cycles are simulated based on a kinetic growth mode.[23] Figures 2(b) shows the simulation and experiment results of final shapes of GaAs after single deposition under growth temperature of 280 °C and BEP of 1.2×10^{-5} Torr. In the simulation, the surface diffusion is assumed isotropic. From the cross-sectional line profiles of the simulated and measured nanorings, the proposed kinetic growth simulation agrees well with the experiment. The simulated and measured nanorings share equal lateral dimension as well as heights of both inner and outer rings. The hole in the center of the nanoring is larger for the simulation than that obtained from the experiment. The holed nanoring is created because of preferred formation of GaAs at the boundary of

the nanodroplets. It should be noted that the size of the nanoholes is about 50 nm, and the AFM probe may not be able to trace the actual nanohole size and shape. What's more, the simulation excludes the effects of GaAs nanostructure height on the diffusion length, which may also be account for the divergence of nanohole size between simulation and experiment.[23]

While the formation mechanism of one layer quantum ring has been well documented. The vertically stacked nanorings by droplet epitaxy has not been investigated. By adopting the kinetic growth mode, the crystallization processes of nanoring formed by multiple deposition of nanodroplets have been simulated. From Figure 1(e1), the initial nanodroplet radius is set as 40 nm. Figure 2(c) and (d) show the three-dimensional surface morphologies and cross profiles of GaAs nanorings after different cycles of droplet epitaxy growth. Figure 2(e) and (f) are the AFM line profiles of GaAs nanoring and three dimension AFM images measured from the nanorings after different cycles of droplet epitaxy growth. From the simulations, the height of ring-structures increases with the increase of deposition cycles, but the radius of ring remain constant during the periodic process. The results are consistent with our experimental observations, as shown in Figure 2(d,e). However, the surface morphologies from the simulations and AFM measurements also demonstrate some distinct differences. Contrary to the simulation, the edge of the nanorings become beveled with increasing deposition cycles. On the other hand, the coin-shaped inner rings evolve into elongated nanodots along $[01\bar{1}]$. Here, the beveled ring morphology with increase of deposition cycles is caused by out-diffusion of the ring material during the growth pauses.[10] The out-diffusion during growth pauses is also accounted for the morphology change of nanorings, which is anisotropic as a result of different diffusion coefficients of Ga adatoms along the $[01\bar{1}]$ and [011] directions.[24]

Figure 3(a) shows magnified AFM images of nanorings grown on samples B, D, E, F, and G. The z-scale of all images is 15 nm. Clearly, the nanoring height increases with increasing deposition cycles as a result of vertically stacked nucleation but with asymmetric configurations. In order to obtain the effects of anisotropic diffusion on the nanorings quantitatively, the dimensions of the nanorings are measured from the AFM images. The measurements of the nanorings are taken along $[01\bar{1}]$ because of the anisotropic shape of the nanorings in this direction. The nanoring dimensions, the higher ring height h_H and lower ring height h_L of the nanorings, as indicated in Figure 3(b), are measured. In the center of the nanorings, nanohole depth, labeled d, is also measured. Figure 3(c) shows the change of nanoring dimension as a function of deposition cycles. With increasing deposition cycles, the inner rings change into dash-like structures, which are aligned in the $[01\bar{1}]$ directions. Both the height h_H and h_L increase with more deposition cycles, suggesting that the vertical stacking of the nanorings has been realized over the entire area of the nanorings. The heights h_H and h_L mainly reflect the vertical dimension of the inner ring (or nano-dashes) formed next to the nanoholes and the outer nanorings, respectively. The depth of nanoholes formed in the center of the nanorings also increase with first few cycles of depositions, but further deposition cycles start to fill the nanoholes instead of drilling in the substrate. On the other hand, the difference between h_H and h_L remains significant. Therefore, the outward diffusion of the droplet is not the only reason for the asymmetry of the nanorings. It was shown earlier that the nucleation of new nanodroplets are off-centered on the preexisting nanorings, which may be attributed to the non-ideal shape of the nanorings. Figure 3(d) shows the density of nanorings as a functions of the droplet epitaxy deposition cycles. The measured density is from 13.6 to 16.4 μm^{-2} for samples B, D, E, F, and G, and thus, increase droplet epitaxy deposition cycles does not notably increase the density of the nanorings, which again confirms the favorable nucleation sites for nanodroplets are the preexisting nanorings and the vertical stacking behavior of droplet epitaxy growth method. This finding is also in good agreement with the results shown in Figure 1(c) and

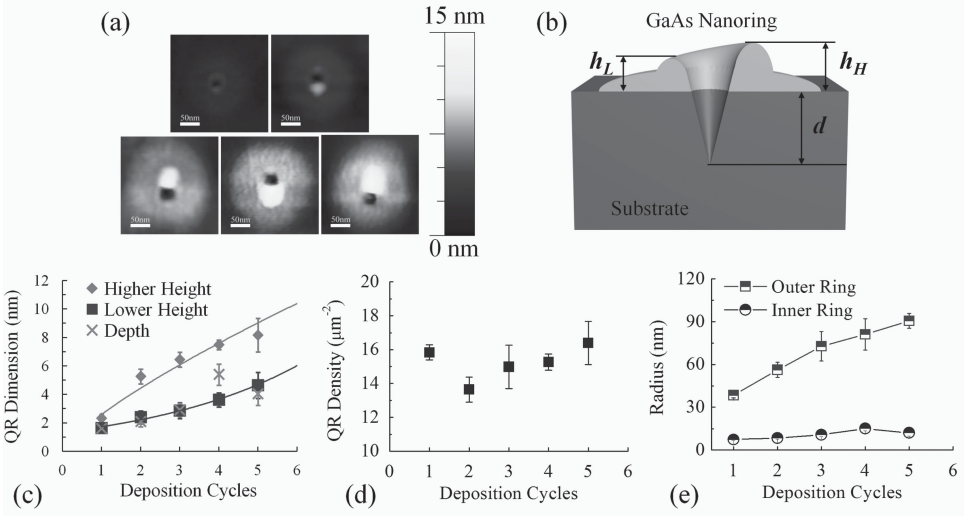

Figure 3. (a) Magnified AFM images of nanorings grown on samples B, D, E, F, and G. The scale bar is 50 nm. The z-scale of all images is 15 nm. (b) Schematic of a GaAs nanoring grown a GaAs substrate. The height of the nanoring (higher ring height h_H and lower ring height h_L) and the depth of the hole in center of the nanoring, d, are indicated. (c) The nanoring dimensions (h_H, h_L, and d) as a function of deposition cycles. (d) The nanoring density as a function of deposition cycles. (e) The outer ring (half-filled squares) and inner ring (half-filled circles) radius as a function of deposition cycles.

Figure 2(e6); the new nanodroplets have nearly one-to-one correlation to the preexisting nanorings. Figure 3(e) shows that the inner nanoring radius remain almost constant while the outer ring radius increases with increasing deposition cycles. When the out-diffusion is excluded in the simulation, the ring diameter is not changing with deposition cycles, which explains the negligible change of inner radius. Compared with inner rings, the Ga out-diffusion is considerable higher for the outer rings.

2.3. Vertically-Correlated Hetero-Droplet Epitaxy

The vertical stacking properties of droplet epitaxy also apply to heterostructures. Three additional samples, I, J and K, were grown. For sample I, $Al_{0.3}Ga_{0.7}$ was deposited at the substrate temperature 280 °C after buffer growth. The alloyed $Al_{0.3}Ga_{0.7}$ droplets were crystallized under As_4 flux (BEP 1.2×10^{-5} Torr) for 1 min. Subsequently, growth pause of 10 minutes was introduced while the As shutter and valve were fully closed. In the end of the growth, 3 ML Ga was supplied. For sample J, $Al_{0.3}Ga_{0.7}As$ buffer was grown instead of GaAs buffer. Ga coverage of 3 ML was supplied on the buffer. Finally, Al and Ga molecular beams equivalent to 3 ML $Al_{0.3}Ga_{0.7}As$ was supplied after crystallization of the Ga droplets and growth pause similar to growth of sample I. Sample K includes an $Al_{0.3}Ga_{0.7}As$ buffer and ten periods of GaAs/ $Al_{0.3}Ga_{0.7}As$ grown by droplet epitaxy under similar conditions as sample I and J. **Figure 4**(a) and (b) show AFM images of the surface morphologies of samples I and J. Interestingly, after formation of $Al_{0.3}Ga_{0.7}As$ (or GaAs) nanorings, following deposition of Ga (or $Al_{0.3}Ga_{0.7}$) nanodroplet also nucleate on the top of the nanorings. Therefore, vertical growth for droplet hetero-epitaxy can also be accomplished, which opens the door to grow advanced nanoheterostructures. Figure 4(c) compares the AFM line profiles of nanohybrids grown on sample I and J. The formation of a nanodroplet sitting on a nanoring is confirmed for both sample. Finally, the nanorings fabricated with ten cycles of GaAs/ $Al_{0.3}Ga_{0.7}As$ droplet hetero-epitaxy is characterized by transmission electron microscopy (TEM), as shown in Figure 4(c) and (d). Figure 4(c) display a nanodot with two regions, A and B. Layered nanostructures are present in B region while absent in A region. The A region can be assigned to a hole observed from the AFM images and the layered nanostructures on the two sides of the A region must be the nanorings. From the high resolution TEM image in Figure 4(d), the layered structures in B region are clearly displayed. The bright and gray layers are assigned as GaAs and $Al_{0.3}Ga_{0.7}As$, respectively. In the TEM images, only eight periods of GaAs and $Al_{0.3}Ga_{0.7}As$ layers were identified even though 10 cycles of droplet hetero-epitaxy was conducted. This can be explained by mis-stacking of nanodroplets during growth. As shown in Figure 4(b), no nanodroplet has been deposited on some of the nanorings. The probability of the occurrence of mis-stacking increases with increasing surface roughness. Similar to droplet homo-epitaxy, the GaAs/ $Al_{0.3}Ga_{0.7}As$ nano-superlattice also haves beveled edges due to longer total diffusion time of nanorings formed earlier. The vertically-correlated hetero-droplet epitaxy can be also employed to form strained heterostructures from mismatched materials,

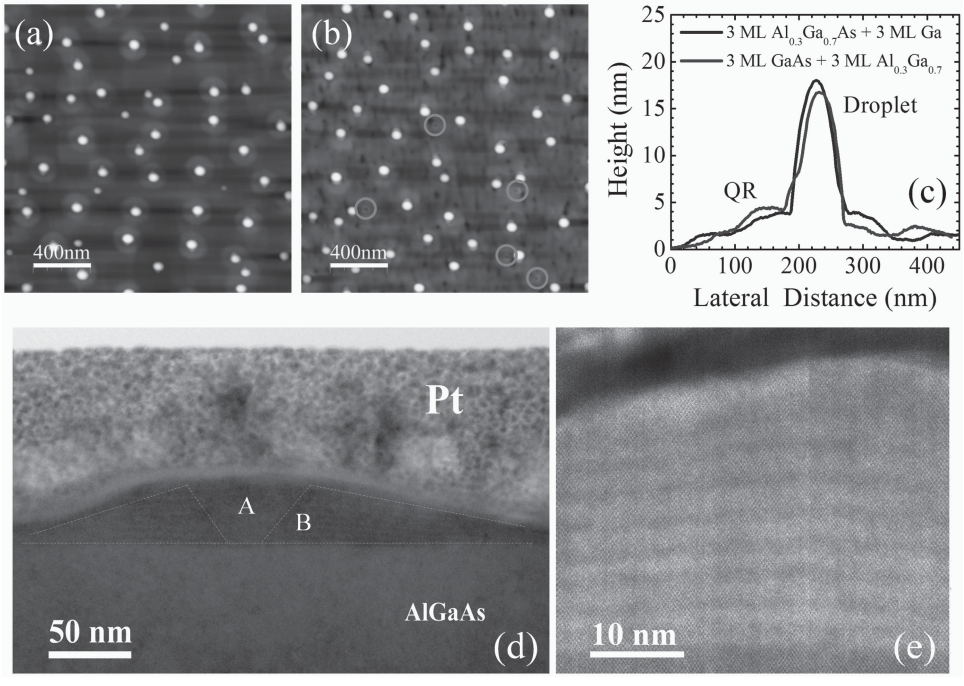

Figure 4. AFM images of $Al_{0.3}Ga_{0.7}As$ nanoring-Ga droplet nanohybrids on sample I (a) and GaAs nanoring-$Al_{0.3}Ga_{0.7}$ droplet nanohybrids on sample J (b). The mis-stacked nanorings are highlighted by circles. (c) AFM line profiles taken from the nanohybrids in (a) and (b). The blue line is the line profile of a typical nanohybrid on sample I and the red line is the line profile of a typical nanohybrid on sample J. (d) A TEM image of a nanoring with interleaving GaAs/$Al_{0.3}Ga_{0.7}$ layers. The nanoring region with layered structures is labeled B while without layered structures labeled A. (e) A high resolution TEM image of the layered GaAs/$Al_{0.3}Ga_{0.7}$ nanoring.

such as InAs/GaAs, since the vertical correlation is mainly governed by the nucleation thermodynamics of the nanodroplets.

3. Conclusion

We have demonstrated vertically correlated growth protocol for Droplet Epitaxy. Vertically stacked multiple nanorings have been fabricated by both homo-Droplet Epitaxy and hetero-Droplet Epitaxy. The vertical growth method is due to preferred nucleation of nanodroplet in the central hole of preexisting nanorings from nucleation thermodynamics analysis. The vertically stacked nanorings can also be understood by the kinetic growth mode. The surface anisotropy of GaAs surface causes non-ideal nanorings with asymmetric shape. The presented growth technique adds another important growth protocol to Droplet Epitaxy. The favored nucleation sites of nanodroplets revealed in this article may also pave the way for lateral growth control of Droplet Epitaxy. The demonstrated technique is capable of fabricating nano-heterostructures, nanosuperlattices, and more complex nanostructures with great potential in nanoelectronics and quantum information devices.

4. Experimental Section

Material Growth: Samples were grown using a molecular beam epitaxy (MBE) system equipped with in situ refection high energy electron diffraction (RHEED). Epi-ready Si-doped GaAs(100) substrates were used. After desorption of the native oxide layer, a buffer layer was grown and the (2×4) surface reconstruction was observed from RHEED patterns. Sequentially, the substrate temperature was ramped down to 280 °C and at the same time, the As cell shutter was closed completely in order to form nanodroplets. After this point, various growth steps were carried out for fabricating different samples. The growth procedures consists of one step or multiple steps of $Ga/Al_{0.3}Ga_{0.7}$ deposition and crystallization with As beam for 60 s. The growth procedures of samples A–K presented in the article are summarized in Table S1.

To study the multiple deposition growth mechanism, the RHEED intensities and patterns were recorded during vertically correlated droplet epitaxy, as shown in Fig. S1. The electron beam was along the $[0\bar{1}1]$ direction. After the buffer growth, the RHEED pattern was (2×4) surface reconstruction. During the Ga deposition, the RHEED intensity decreased immediately and the streaky patterns disappeared, as shown in Figure S1 and Figure S2. The reduced RHEED intensity is attributed to reduced reflection of the electrons from the Ga nanodroplets. The transformation of As-rich surface to Ga-rich surface has made the surface reconstruction change from (2×4) to (2×1). After crystallization of Ga nanodroplets, spotty features appeared in the RHEED patterns, which indicated formation of three-dimensional GaAs nanostructures. In addition, the RHEED intensity increased after crystallization of Ga nanodroplets due to restore of the crystalline surface. The evolutions of RHEED patterns were found to be the same for subsequent Ga depositions and crystallizations with As, which suggested similar growth dynamics.

Characterization: The surface morphologies of the samples were characterized by an Veeco 3100 atomic force microscopy under ambient conditions. The cross-sectional transmission electron microscopy images were taken by a FEI Titan 80–300 transmission electron microscope.

Supporting Information

Supporting Information is available from the Wiley Online Library or from the author.

Acknowledgements

J. Wu, Y. Hirono, and X. Li contributed equally to this work. This work was supported in part by the National Science Foundation through EPSCoR Grant No. EPS1003970, the National Basic Research Program (973) of China (2013CB933301), the NRF through Grant No. 2011–0030821, and the National Natural Science Foundation of China through Grant NSFC-51272038 and NSFC-61204060.

Received: June 14, 2013
Revised: July 9, 2013
Published online: August 12, 2013

[1] A. Martí, E. Antolín, C. R. Stanley, C. D. Farmer, N. López, P. Díaz, E. Cánovas, P. G. Linares, A. Luque, *Phys. Rev. Lett.* **2006**, *97*, 247701.
[2] Y. He, Y. He, Y. Wei, D. Wu, M. Atatüre, C. Schneider, S. Höfling, M. Kamp, C. Lu, J. Pan, *Nature Nanotechnol.* **2013**, *8*, 213.
[3] J. Wu, D. Shao, V. G. Dorogan, A. Z. Li, S. Li, E. A. Decuir, M. O. Manasreh, Z. M. Wang, Y. I. Mazur, G. J. Salamo, *Nano Lett.* **2010**, *10*, 1512–1516.
[4] H. Liu, T. Wang, Q. Jiang, R. Hogg, F. Tutu, F. Pozzi, A. Seeds, *Nat. Photon.* **2011**, *5*, 416–419.
[5] C. Livermore, C. Crouch, R. Westervelt, K. Campman, A. Gossard, *Science* **1996**, *274*, 1332.
[6] W. Gao, P. Fallahi, E. Togan, J. Miguel-Sanchez, A. Imamoglu, *Nature.* **2012**, *491*, 426–430.
[7] D. P. Kumah, S. Shusterman, Y. Paltiel, Y. Yacoby, R. Clarke, *Nature Nanotechnol.* **2009**, *4*, 835–838.
[8] L. Wang, A. Rastelli, S. Kiravittaya, M. Benyoucef, O. G. Schmidt, *Adv. Mater.* **2009**, *21*, 2601–2618.
[9] M. Hocevar, G. Immink, M. Verheijen, N. Akopian, V. Zwiller, L. Kouwenhoven, E. Bakkers, *Nature Commun.* **2012**, *3*, 1266.
[10] C. Somaschini, S. Bietti, N. Koguchi, S. Sanguinetti, *Nano Lett.* **2009**, *9*, 3419–3424.
[11] Z. M. Wang, K. Holmes, Y. I. Mazur, K. A. Ramsey, G. J. Salamo, *Nanoscale Res. Lett.* **2006**, *1*, 57–61.
[12] C. Somaschini, S. Bietti, A. Scaccabarozzi, E. Grilli, S. Sanguinetti, *Cryst. Growth Des.* **2012**, *12*, 1180–1184.
[13] T. Mano, T. Kuroda, S. Sanguinetti, T. Ochiai, T. Tateno, J. Kim, T. Noda, M. Kawabe, K. Sakoda, G. Kido, N. Koguchi, *Nano Lett.* **2005**, *5*, 425–428.
[14] M. K. Yakes, C. D. Cress, J. G. Tischler, A. S. Bracker, *ACS Nano* **2010**.
[15] M. Creasey, J. Lee, Z. Wang, G. Salamo, X. Li, *Nano Lett.* **2012**.
[16] J. H. Lee, Z. M. Wang, N. W. Strom, Y. I. Mazur, G. J. Salamo, *Appl. Phys. Lett.* **2006**, *89*, 202101.
[17] M. Schmidbauer, S. Seydmohamadi, D. Grigoriev, Z. M. Wang, Y. I. Mazur, P. Schäfer, M. Hanke, R. Köhler, G. J. Salamo, *Phys. Rev. Lett.* **2006**, *96*, 066108.
[18] J. Tersoff, C. Teichert, M. G. Lagally, *Phys. Rev. Lett.* **1996**, *76*, 1675.
[19] Z. M. Wang, B. L. Liang, K. A. Sablon, G. J. Salamo, *Appl. Phys. Lett.* **2007**, *90*, 113120.
[20] The contact angle of a Ga nanodroplet has been estimate to be 70° (see ref 13). Due to the difference in the growth conditions, the free energies and thus the contact angle α may change. Therefore, in the calculation, three additional values, 50°, 60°, and 80°, of the contact angle α have been used.
[21] R. N. Wenzel, *Industrial Engin. Chem.* **1936**, *28*, 988–994.
[22] L. Feng, Y. Song, J. Zhai, B. Liu, J. Xu, L. Jiang, D. Zhu, *Angew. Chem.* **2003**, *115*, 824–826.
[23] X. L. Li, G. W. Yang, *J. Appl. Phys.* **2009**, *105*, 103507.
[24] C. Somaschini, S. Bietti, A. Fedorov, N. Koguchi, S. Sanguinetti, *Nanoscale Res. Lett.* **2010**, *5*, 1865–1867.